Hee-Jin Jun,[1] Yagini Joshi,[1] Yuvraj Patil,[1] Robert C. Noland,[2] and Ji Suk Chang[1]

NT-PGC-1α Activation Attenuates High-Fat Diet–Induced Obesity by Enhancing Brown Fat Thermogenesis and Adipose Tissue Oxidative Metabolism

Diabetes 2014;63:3615–3625 | DOI: 10.2337/db13-1837

The transcriptional coactivator peroxisome proliferator–activated receptor γ coactivator (PGC)-1α and its splice variant N terminal (NT)-PGC-1α regulate adaptive thermogenesis by transcriptional induction of thermogenic and mitochondrial genes involved in energy metabolism. We previously reported that full-length PGC-1α (FL-PGC-1α) is dispensable for cold-induced nonshivering thermogenesis in FL-PGC-1α$^{-/-}$ mice, since a slightly shorter but functionally equivalent form of NT-PGC-1α (NT-PGC-1α^{254}) fully compensates for the loss of FL-PGC-1α in brown and white adipose tissue. In the current study, we challenged FL-PGC-1α$^{-/-}$ mice with a high-fat diet (HFD) to investigate the effects of diet-induced thermogenesis on HFD-induced obesity. Despite a large decrease in locomotor activity, FL-PGC-1α$^{-/-}$ mice exhibited the surprising ability to attenuate HFD-induced obesity. Reduced fat mass in FL-PGC-1α$^{-/-}$ mice was closely associated with an increase in body temperature, energy expenditure, and whole-body fatty acid oxidation (FAO). Mechanistically, FL-PGC-1α$^{-/-}$ brown adipose tissue had an increased capacity to oxidize fatty acids and dissipate energy as heat, in accordance with upregulation of thermogenic genes UCP1 and DIO2. Furthermore, augmented expression of FAO and lipolytic genes in FL-PGC-1α$^{-/-}$ white adipose tissue was highly correlated with decreased fat storage in adipose tissue. Collectively, our data highlight a protective effect of NT-PGC-1α on diet-induced obesity by enhancing diet-induced thermogenesis and FAO.

Obesity, a primary risk factor for type 2 diabetes, is characterized by an expansion of adipose tissue mass due to chronic imbalance between energy intake and expenditure. The recent rise in obesity has greatly increased interest in brown adipose tissue (BAT) as a potential therapeutic target to increase energy expenditure (EE) and treat obesity, given that BAT has an ability to oxidize large amounts of lipids and glucose and to dissipate the energy generated by fuel oxidation as heat through uncoupling protein 1 (UCP1) (1–5). Recent studies using positron emission tomography/computed tomography with ^{18}F-fluorodeoxyglucose have clearly shown that adult humans contain substantial depots of metabolically active brown fat (6–11), which is inversely correlated with BMI, age, and diabetes status (6,12).

In rodents and small mammals, BAT-mediated thermogenesis is important for maintenance of core body temperature at temperatures below thermoneutrality (cold-induced nonshivering thermogenesis) (13). Substantial evidence has also demonstrated that BAT thermogenesis plays a crucial role in the regulation of energy balance by burning off excess calories (diet-induced thermogenesis)

[1]Laboratory of Nutrient Sensing and Adipocyte Signaling, Pennington Biomedical Research Center, Baton Rouge, LA
[2]Laboratory of Skeletal Muscle Metabolism, Pennington Biomedical Research Center, Baton Rouge, LA
Corresponding author: Ji Suk Chang, jisuk.chang@pbrc.edu.

Received 3 December 2013 and accepted 16 May 2014.
This article contains Supplementary Data online at http://diabetes.diabetesjournals.org/lookup/suppl/doi:10.2337/db13-1837/-/DC1.

(14–18). Cold or increased caloric intake stimulates the sympathetic nervous system, leading to the release of norepinephrine that activates β-adrenergic receptors on BAT (19). Mice lacking β-adrenergic receptors are obese and more sensitive to high-fat diet (HFD)–induced obesity due to impaired BAT thermogenesis (16). Similarly, BAT dysfunction induced by UCP1 deficiency increases susceptibility to diet-induced obesity (18,20,21). On the other hand, enhancement of thermogenic activity by UCP1 overexpression or by BAT activators such as cold exposure, β-adrenergic receptor agonists, bile acids, and fibroblast growth factor 21 reduces dietary and genetic obesity (22–25).

Peroxisome proliferator–activated receptor γ coactivator (PGC)-1α is a master regulator of BAT thermogenesis (26). PGC-1α coactivates various nuclear receptors for transcriptional induction of UCP1 and other mitochondrial genes involved in mitochondrial biogenesis and oxidative metabolism (27). Previously, we have shown that N terminal (NT)-PGC-1α, a short isoform of PGC-1α produced by alternative splicing of the PGC-1α gene, also plays a crucial role in BAT thermogenesis (28–30). Forced expression of NT-PGC-1α in cultured PGC-1α$^{-/-}$ brown adipocytes increases thermogenic capacity by transcriptional induction of thermogenic and mitochondrial genes (28,29,31). In agreement with in vitro data, full-length (FL)-PGC-1α$^{-/-}$ mice expressing a slightly shorter but functionally equivalent form of NT-PGC-1α (NT-PGC-1α^{254}) have the ability to activate a brown fat thermogenic program in the absence of FL-PGC-1α and to maintain body temperature during a cold challenge (30). In contrast, PGC-1α$^{-/-}$ mice deficient in both PGC-1α and NT-PGC-1α are unable to defend against cold stress due to impaired BAT thermogenesis (32). Prolonged cold exposure or β-adrenergic receptor activation also induces remodeling of white adipose tissue by increasing brown-like (beige) adipocytes (33,34). Elevated expression of PGC-1α and NT-PGC-1α in beige adipocytes promotes the transcription of UCP1 and mitochondrial genes, thus increasing thermogenic and oxidative capacity (26,35). FL-PGC-1α$^{-/-}$ white adipose tissue also undergoes browning as evidenced by an increase in UCP1-positive multilocular cells (30), suggesting that NT-PGC-1α^{254} is sufficient to activate a thermogenic transcriptional program in white adipocytes as well. Together, NT-PGC-1α is an important regulator of adaptive thermogenesis and oxidative metabolism in both brown and white adipocytes.

The main objective of the current study was to investigate how NT-PGC-1α regulates energy metabolism in brown and white adipose tissue under the HFD condition. Here, we report that FL-PGC-1α$^{-/-}$ mice are resistant to HFD-induced obesity by oxidizing more fat and expending more energy as heat.

RESEARCH DESIGN AND METHODS

Animals and Diets

FL-PGC-1α$^{-/-}$ mice have previously been described (30,36). All mice were housed on a 12-h light/12-h dark cycle at 22–23°C. At the age of 7–8 weeks, male wild-type (WT) and FL-PGC-1α$^{-/-}$ mice (n = 8 per group) were singly housed and provided a standard chow (13% fat in kilocalories) (LabDiet, St. Louis, MO) or an HFD (45% fat in kilocalories) (D12451; Research Diets, Inc., New Brunswick, NJ) ad libitum for 16 weeks. Their body weight and food intake were monitored every week. All animal experiments were conducted according to procedures reviewed and approved by the Pennington Biomedical Research Center Institutional Animal Care and Use Committee on the basis of guidelines established by the National Research Council, the Animal Welfare Act, and the Public Health Service Policy on the humane care and use of laboratory animals.

Metabolic Studies

For insulin tolerance test, WT and FL-PGC-1α$^{-/-}$ mice were fasted for 5 h and injected with insulin (0.75 units/kg body wt i.p.), whereas for glucose tolerance test, mice were fasted for 16 h and injected with a glucose bolus (2 g/kg body wt i.p.). Tail blood glucose levels were measured at indicated time points using a glucometer (OneTouch; LifeScan). Fasting serum levels of insulin and triglyceride were measured with a rat/mouse insulin ELISA kit (Millipore, Billerica, MA) and Triglyceride Colorimetric Assay kit (Cayman Chemical, Ann Arbor, MI), respectively.

Body Composition and Indirect Calorimetric Analysis

Body composition was determined by nuclear magnetic resonance using a Bruker Mouse Minispec (Bruker Optics, Billerica, MA). For conducting metabolic phenotyping, WT and FL-PGC-1α$^{-/-}$ mice fed with HFD for 10 weeks were weighed and their body composition was determined prior to transfer into indirect calorimetry chambers. After a 24-h acclimation period, each mouse was monitored for 72 h on HFD for determination of V_{O_2} and V_{CO_2} using a Comprehensive Lab Animal Monitoring System (Columbus Instruments, Columbus, OH). Physical activity was measured using an Opto M3 sensor system while the mice were in the chamber.

Western Blot Analysis

Whole-cell extracts were prepared from tissues or brown adipocytes by homogenization in lysis buffer (29) and subjected to Western blot analysis using the following antibodies: anti–PGC-1α (28), anti-FAS, anti-SCD1, anti-actin (Santa Cruz, Dallas, TX), anti–α-tubulin, and anti-GAPDH (Abcam, Cambridge, MA).

Quantitative Real-Time PCR Analysis

Total RNA from tissues or brown adipocytes was reverse transcribed for quantitative real-time PCR analysis as previously described (29,30). Relative expression of mRNAs was determined after normalization to cyclophilin by the standard curve method.

Generation and Culture of Brown Adipocyte Cell Lines

Brown preadipocytes were isolated from interscapular BAT of newborn WT and FL-PGC-1α$^{-/-}$ mice by collagenase

digestion and immortalized by infection with SV40T antigen-expressing retrovirus as previously described (28). PGC-1α$^{-/-}$ brown preadipocytes expressing pBABE, NT-PGC-1α, or NT-PGC-1α^{254} were generated and differentiated as previously described (29).

Cellular and Tissue O_2 Consumption Rates

Oxygen consumption rates of BAT were monitored using freshly isolated BAT as previously described (37). Briefly, BAT explants from male WT and FL-PGC-1α$^{-/-}$ mice (n = 5 per group) fed HFD for 13 weeks were minced into small pieces. Approximately 5 mg minced BAT was then placed in a magnetically stirred respirometric chamber of the OROBOROS Oxygraph-2k (Oroboros Instruments, Innsbruck, Austria) containing the respiration buffer. Oxygen consumption was measured in duplicate after injection of malate/pyruvate, rotenone/succinate, glycerol-3-phosphate, or malate/palmitoyl carnitine, followed by addition of oligomycin and antimycin A. Respiratory measurements were normalized by the tissue weight. For the oxygen consumption rate (OCR) of brown adipocytes, 10^6 cells were placed in a respirometric chamber containing the culture medium. OCR measurements (n = 6–8 per group) were obtained at baseline and after injection of oligomycin and antimycin A. The value of basal respiration, uncoupled respiration, and nonmitochondrial respiration was determined as described in the Oroboros Operator's Manual.

Fatty Acid Oxidation Assay

Rates of palmitate oxidation were measured as previously described (38) with a slight modification. In brief, freshly isolated BAT was homogenized in SET buffer. Quadruple homogenate incubations were performed in reaction buffer containing [1-^{14}C]palmitate (0.65 μCi/mL) for 30 min at 37°C and terminated with the addition of 70% perchloric acid. Complete ($^{14}CO_2$ trapped in 1 N NaOH) and incomplete (^{14}C-acid–soluble metabolites) oxidation was measured by scintillation.

Histology and Adipose Cell Size Analysis

Tissue samples were fixed in 10% neutral-buffered formalin, embedded in paraffin, sectioned (5 μm), and then stained with hematoxylin–eosin (H-E). H-E–stained paraffin sections of adipose tissue were scanned using a Hamamatsu NanoZoomer slide scanner (Hamamatsu Phototonics, Hamamatsu, Japan) and analyzed for adipocyte size using Fiji software (39). The Analyze Particles tool was used to identify adipocytes with sizes from 500 to 8,000 μm^2.

Lipolysis Assay

Inguinal and epididymal adipose tissues were freshly isolated from WT and FL-PGC-1α$^{-/-}$ mice (n = 5 per group) fed HFD for 13 weeks. Adipose tissue explants were minced and incubated with collagenase in Krebs-Henseleit buffer containing 5 mmol/L glucose and 2% BSA at 37°C with gentle shaking. Isolated adipocytes were filtered through a nylon mesh and washed with Krebs-Henseleit buffer. Lipolytic activity was measured in triplicate by incubating equal amounts of adipocytes at 37°C for 2 h in the absence or presence of isoproterenol (100 nmol/L). Glycerol release was determined by absorbance at 320 nm after incubating aliquots (25 μL) of the infranatant with 125 μL glycerol assay buffer (pH 9.5) containing 1 mg/mL β-nicotinamide adenine dinucleotide, 1.8 mmol/L ATP, GAPDH, and glycerokinase for 40 min.

Tissue Triglyceride Analysis

Tissue samples (40–60 mg) were homogenized in the Standard Diluent Assay Reagent provided by a Triglyceride Colorimetric Assay kit (Cayman Chemical), and triglyceride concentrations were measured as described in the manufacturer's instructions.

Statistical Analysis

Data are presented as mean ± SEM. Student t test was used to compare the differences between groups. Values of $P < 0.05$ were considered statistically significant. EE (kilojoules per hour) was adjusted for independent variables (lean mass, fat mass, and activity) using multiple regression analysis (JMP Pro 11 software) as previously described (40–42).

RESULTS

HFD-Induced Obesity Is Attenuated in FL-PGC-1α$^{-/-}$ Mice

The FL-PGC-1α$^{-/-}$ mouse lacks FL-PGC-1α but retains a slightly shorter but functionally equivalent form of NT-PGC-1α (NT-PGC-1α^{254}) (Fig. 1*A* and Supplementary Fig. 1*B*). During a cold challenge, FL-PGC-1α$^{-/-}$ mice are able to activate cold-induced thermogenesis, since NT-PGC-1α^{254} protein induces thermogenic gene expression and mitochondrial biogenesis in BAT (30). Given that BAT activity also regulates energy balance in rodents by burning off excess calories, we examined the ability of FL-PGC-1α$^{-/-}$ mice to activate diet-induced thermogenesis in response to HFD and its effect on diet-induced obesity by placing WT and FL-PGC-1α$^{-/-}$ mice on a standard chow or HFD for 16 weeks.

On the chow diet, WT and FL-PGC-1α$^{-/-}$ mice exhibited comparable weight gains (Fig. 1*B*) and similar body composition (Fig. 1*C*). When placed on HFD, FL-PGC-1α$^{-/-}$ mice displayed a small, but not statistically significant, reduction in weight gains compared with WT mice (Fig. 1*B*). However, FL-PGC-1α$^{-/-}$ mice showed a significant reduction in adiposity over the course of high-fat feeding (Fig. 1*E*). After 16 weeks of HFD, FL-PGC-1α$^{-/-}$ mice exhibited a large decrease in fat mass compared with WT mice (Fig. 1*C*), and weights of inguinal, epididymal, and retroperitoneal fat depots were ~30% lower than those of WT mice (Fig. 1*F*). In addition, FL-PGC-1α$^{-/-}$ mice exhibited a significant reduction in liver weights. The serum triglyceride levels were 14% lower in FL-PGC-1α$^{-/-}$ mice, although this difference did not reach statistical significance (P = 0.09) (Fig. 1*G*). The observed reduction in fat mass in FL-PGC-1α$^{-/-}$ mice was not due to alteration in food intake (Fig. 1*D*),

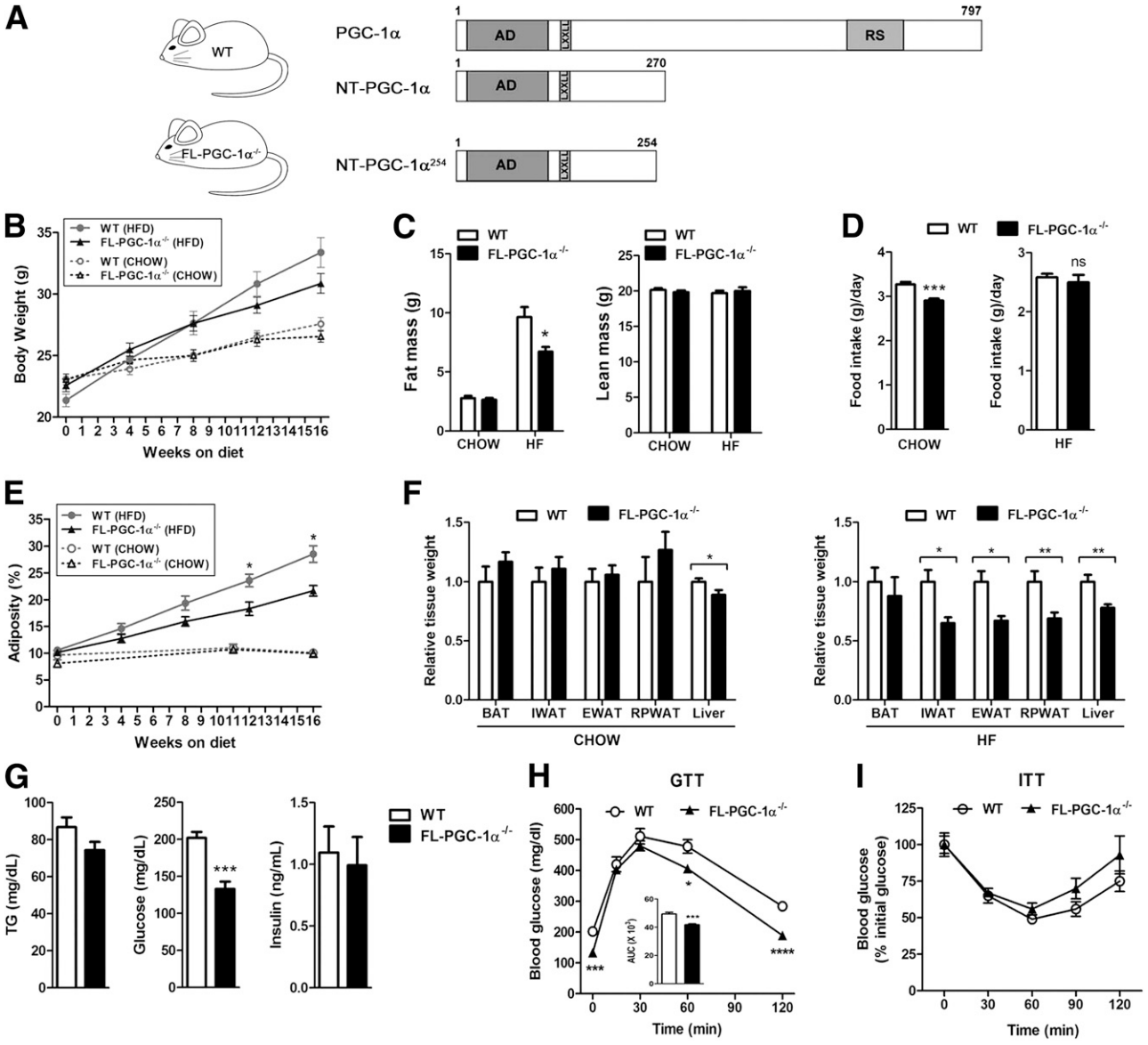

Figure 1—FL-PGC-1α$^{-/-}$ mice display a significant reduction in adiposity on HFD. *A*: Schematic diagram of WT and FL-PGC-1α$^{-/-}$ mice expressing PGC-1α/NT-PGC-1α and NT-PGC-1α^{254}, respectively. AD, activation domain; RS, arginine/serine-rich domain. *B*: Body weight of male WT and FL-PGC-1α$^{-/-}$ mice on either chow or HFD (n = 8 per group). *C*: Body composition of WT and FL-PGC-1α$^{-/-}$ mice determined by nuclear magnetic resonance after 16 weeks of either chow or HFD feeding (HF) (n = 8 per group). *D*: Average food intake of WT and FL-PGC-1α$^{-/-}$ mice on either chow or HFD (n = 8 per group). Food intake was monitored once a week for 16 weeks and was expressed as grams per day per mouse. ns, not significant. *E*: Percent body fat during chow or HFD feeding for 16 weeks. *F*: Relative weights of BAT, inguinal white adipose tissue (IWAT), epididymal white adipose tissue (EWAT), and retroperitoneal white adipose tissue (RPWAT) fat pads and livers from WT and FL-PGC-1α$^{-/-}$ mice fed either chow or HFD. *G*: Fasting serum triglyceride (TG), glucose, and insulin levels in WT and FL-PGC-1α$^{-/-}$ mice fed HFD. Serum TG levels were measured from mice fed HFD for 16 weeks in a 5-h–fasted state (n = 8 per group). Blood glucose and insulin levels were measured from WT and FL-PGC-1α$^{-/-}$ mice fed HFD for 13 weeks in the overnight-fasted state (n = 8 per group). *H*: Glucose tolerance test in WT and FL-PGC-1α$^{-/-}$ mice fed HFD for 13 weeks in the overnight-fasted state (n = 8 per group). Histograms represent the areas under the glucose curve. *I*: Insulin tolerance test in WT and FL-PGC-1α$^{-/-}$ mice fed HFD for 12 weeks in the 5-h–fasted state (n = 8 per group). All data are presented as the mean ± SEM. *P < 0.05, **P < 0.01, ***P < 0.001, ****P < 0.0001 determined by Student t test.

suggesting alternations in energy metabolism. Furthermore, at thermoneutral conditions that minimize mild cold-induced sympathetic activity, FL-PGC-1α$^{-/-}$ mice exhibited lower adiposity than WT mice on HFD (Supplementary Fig. 2*C* and *D*), indicating a potential contribution of HFD-induced BAT thermogenesis to the attenuation of diet-induced obesity.

Since decreased adiposity is often associated with improved glucose homeostasis, we investigated whether decreased fat mass in FL-PGC-1α$^{-/-}$ mice would lead to improvement in glucose handling and insulin sensitivity. Fasting blood glucose levels were significantly lower in HFD-fed FL-PGC-1α$^{-/-}$ mice compared with WT mice, whereas corresponding insulin levels were not different

between groups (Fig. 1*G*). During glucose tolerance test, FL-PGC-1α$^{-/-}$ mice displayed significantly improved glucose tolerance, resulting in a 15% reduction in area under the glucose curve (Fig. 1*H*). However, FL-PGC-1α$^{-/-}$ mice showed similar glucose disposal rates after insulin administration (Fig. 1*I*).

FL-PGC-1α$^{-/-}$ Mice Exhibit Increased Energy Expenditure and Greater Reliance on Fat Oxidation

To determine whether FL-PGC-1α$^{-/-}$ mice have increased EE on HFD, we examined whole-body O_2 consumption and CO_2 production in WT and FL-PGC-1α$^{-/-}$ mice for 3 days. Because body composition (Fig. 1*C*) and locomotor activity (Fig. 2*B*) were significantly different between WT and FL-PGC-1α$^{-/-}$ mice, EE was statistically adjusted for lean mass, fat mass, and activity using multiple regression analysis (40–42) (Supplementary Table 1). In line with the lean phenotype, FL-PGC-1α$^{-/-}$ mice displayed higher EE than WT mice (Fig. 2*A*). Moreover, FL-PGC-1α$^{-/-}$ mice exhibited a greater reliance on fat oxidation, as reflected by lower respiratory exchange ratio (Fig. 2*C*).

Given that HFD activates norepinephrine-induced thermogenesis in BAT (14,15), we investigated whether BAT thermogenesis contributes to the increased EE in FL-PGC-1α$^{-/-}$ mice. Indeed, FL-PGC-1α$^{-/-}$ mice had higher core body temperature than WT mice on HFD (Fig. 2*D*). Similarly, when placed at 4°C for 48 h, FL-PGC-1α$^{-/-}$ mice were slightly hyperthermic (Fig. 2*E*). Together, these results suggest that FL-PGC-1α$^{-/-}$ mice burn more fat compared with WT mice and expend more energy through BAT thermogenesis.

Increased BAT Thermogenic Activity in FL-PGC-1α$^{-/-}$ Mice

In HFD-fed WT mice, PGC-1α protein was below the detectable level in BAT, whereas NT-PGC-1α protein was expressed at low but detectable levels (Fig. 3*B*). On the contrary, NT-PGC-1α^{254} protein was abundantly expressed in FL-PGC-1α$^{-/-}$ BAT mice (Fig. 3*B*). It should be noted that this increase in protein levels was not due to increased mRNA expression (Fig. 3*A*), as reported previously (30). Given that PGC-1α and NT-PGC-1α regulate the expression of thermogenic, mitochondrial, and metabolic genes, we assessed gene expression profiles in WT and FL-PGC-1α$^{-/-}$ BAT mice. The expression of key thermogenic genes UCP1 and DIO2, which are indispensable for cold- and diet-induced BAT thermogenesis (2,18,43–45), was significantly increased in FL-PGC-1α$^{-/-}$ BAT mice compared with WT controls (Fig. 3*C*). However, the upregulation of UCP1 and DIO2 was not observed in BAT from chow-fed FL-PGC-1α$^{-/-}$ mice (Supplementary Fig. 3), indicating that high-fat feeding elevates the expression of UCP1 and DIO2 in FL-PGC-1α$^{-/-}$ BAT mice. Transcript levels of mitochondrial OXPHOS, fatty acid oxidation (FAO), lipolysis, and glucose uptake genes were comparable between WT and FL-PGC-1α$^{-/-}$ BAT mice (Fig. 3*C*).

To determine the thermogenic activity of FL-PGC-1α$^{-/-}$ BAT, we assessed oxygen consumption rates of BAT explants from FL-PGC-1α$^{-/-}$ mice in the presence of multiple respiratory substrates. We measured uncoupled respiration that represents oxygen consumption linked to UCP1-mediated thermogenesis. Approximately 80–90% of substrate-responsive oxygen consumption relied on

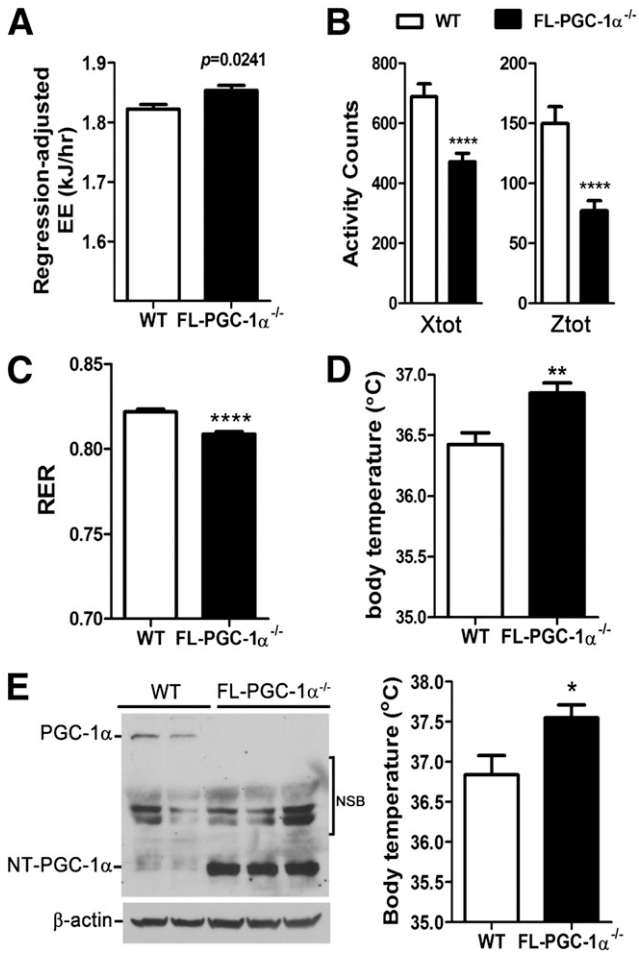

Figure 2—Increased EE, thermogenesis, and fat oxidation in FL-PGC-1α$^{-/-}$ mice. *A*: EE of WT and FL-PGC-1α$^{-/-}$ mice fed HFD (n = 7 per group). EE (kilojoules per hour) was calculated by the equation $Vo_2 \times [3.815 + (1.232 \times \text{respiratory quotient})] \times 4.187$ from repeated measures of oxygen consumption collected at 18-min intervals for 3 days. EE values were then normalized using multiple regression analysis (JMP Pro 11 software) to adjust for differences in body composition (lean mass and fat mass) and activity between WT and FL-PGC-1α$^{-/-}$ mice. Histograms represent the least square means of EE adjusted for lean mass, fat mass, and activity. For additional analysis details, see Supplementary Table 1. *B*: Voluntary activity of WT and FL-PGC-1α$^{-/-}$ mice on HFD. Xtot, ambulatory activity; Ztot, rearing activity. *C*: Average respiratory exchange ratio (RER) of WT and FL-PGC-1α$^{-/-}$ mice on HFD. *D*: Body temperature of WT and FL-PGC-1α$^{-/-}$ mice (n = 8 per group) on HFD. Core body temperature was measured using a MicroTherma thermometer with an RET-3 mouse rectal probe. *E*: Cold-induced BAT thermogenesis. Western blot analysis of PGC-1α/NT-PGC-1α and NT-PGC-1α^{254} proteins in brown fat extracts from WT and FL-PGC-1α$^{-/-}$ mice placed at 4°C, respectively (*left*). NSB, nonspecific bands. Body temperature of 10- to 12-week-old WT and FL-PGC-1α$^{-/-}$ mice placed at 4°C for 48 h (n = 8–9 per group) (*right*). All data are presented as the mean ± SEM. *P < 0.05, **P < 0.01, ****P < 0.0001 determined by Student t test.

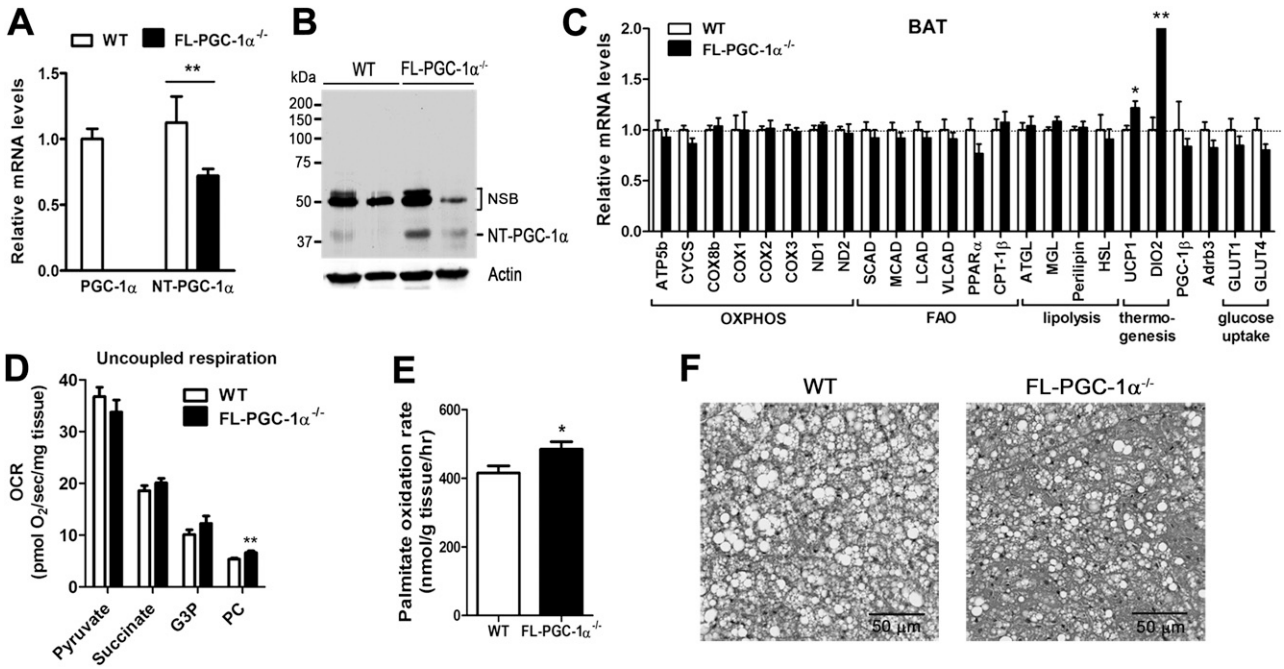

Figure 3—Increased expression of UCP1 and DIO2 and enhanced mitochondrial uncoupling in FL-PGC-1α$^{-/-}$ BAT. *A*: Quantitative real-time PCR analysis of PGC-1α/NT-PGC-1α and NT-PGC-1α^{254} mRNA in BAT from WT and FL-PGC-1α$^{-/-}$ mice fed HFD, respectively. *B*: Protein levels of PGC-1α/NT-PGC-1α and NT-PGC-1α^{254} in BAT from WT and FL-PGC-1α$^{-/-}$ mice fed HFD, respectively. NSB represents nonspecific bands. *C*: Quantitative real-time PCR analysis of mitochondrial OXPHOS, FAO, lipolytic, glucose uptake, and thermogenic genes in BAT from WT and FL-PGC-1α$^{-/-}$ mice fed HFD (n = 8 per group). *D*: Oxygen consumption rates of minced BAT from WT and FL-PGC-1α$^{-/-}$ mice fed HFD for 13 weeks. Uncoupled respiration linked to UCP1-mediated proton leak was measured by injection of oligomycin to inhibit ATP synthesis-coupled respiration in the presence of different substrates: 2 mmol/L malate and 5 mmol/L pyruvate, 1 μmol/L rotenone and 10 mmol/L succinate, 10 mmol/L glycerol-3-phosphate (G3P), and 2 mmol/L malate and 30 μmol/L palmitoyl carnitine (PC). sec, second. *E*: FAO of [^{14}C]palmitate in BAT homogenates from WT and FL-PGC-1α$^{-/-}$ mice (n = 6 per group). Total palmitate oxidation was determined by measuring $^{14}CO_2$ production and ^{14}C-labeled acid soluble metabolites. hr, hour. *F*: Representative images of H-E–stained sections of BAT from WT and FL-PGC-1α$^{-/-}$ mice fed HFD for 16 weeks. Scale bar: 50 μm. All data are presented as the mean ± SEM. *P < 0.05, **P < 0.01 determined by Student t test.

uncoupled respiration in WT and FL-PGC-1α$^{-/-}$ BAT (data not shown). In the presence of pyruvate, succinate, and glycerol-3-phosphate, uncoupled respiration was comparable between WT and FL-PGC-1α$^{-/-}$ BAT mice (Fig. 3*D*). However, palmitoyl carnitine–responsive uncoupled respiration was significantly higher (24%) in FL-PGC-1α$^{-/-}$ BAT, suggesting that FL-PGC-1α$^{-/-}$ BAT prefers fatty acids as a respiratory substrate for thermogenesis. In line with this, oxidation rates of palmitate were significantly higher in BAT homogenates from FL-PGC-1α$^{-/-}$ mice (Fig. 3*E*). Histology also revealed a substantial decrease in the accumulation of lipid droplets in FL-PGC-1α$^{-/-}$ BAT mice compared with WT controls (Fig. 3*F*).

NT-PGC-1α Activation Increases Thermogenic Capacity in Brown Adipocytes

For determination of whether the increased thermogenic activity of FL-PGC-1α$^{-/-}$ BAT is cell autonomous, immortalized WT, FL-PGC-1α$^{-/-}$, and PGC-1α$^{-/-}$ brown preadipocytes were differentiated in vitro. Given that HFD-induced sympathetic stimulation activates cAMP signaling in BAT (19), these brown adipocytes were treated with vehicle or dibutyryl cAMP for 6 h. As previously shown (28), cAMP highly induced PGC-1α, NT-PGC-1α, and NT-PGC-1α^{254} in brown adipocytes (Fig. 4*A*). The basal mRNA levels of thermogenic and mitochondrial genes were higher in WT and FL-PGC-1α$^{-/-}$ brown adipocytes compared with PGC-1α$^{-/-}$ controls (Fig. 4*B*). cAMP further induced expression of UCP1 and DIO2 with a larger increase in WT and FL-PGC-1α$^{-/-}$ brown adipocytes than PGC-1α$^{-/-}$ controls (Fig. 4*B*). In agreement with gene expression data, WT and FL-PGC-1α$^{-/-}$ brown adipocytes displayed higher basal levels of total and uncoupled respiration than PGC-1α$^{-/-}$ controls (Fig. 4*C*). Treatment with cAMP largely elevated total and uncoupled respiration in WT and FL-PGC-1α$^{-/-}$ brown adipocytes but had little effect on the respiration in PGC-1α$^{-/-}$ brown adipocytes (Fig. 4*C*). In particular, cAMP-stimulated uncoupled respiration was higher in FL-PGC-1α$^{-/-}$ brown adipocytes compared with WT controls.

To further confirm the direct effect of NT-PGC-1α on the activation of a brown fat thermogenic program, we expressed NT-PGC-1α and NT-PGC-1α^{254} in PGC-1α$^{-/-}$ brown adipocytes. NT-PGC-1α and NT-PGC-1α^{254} highly induced the expression of thermogenic and mitochondrial

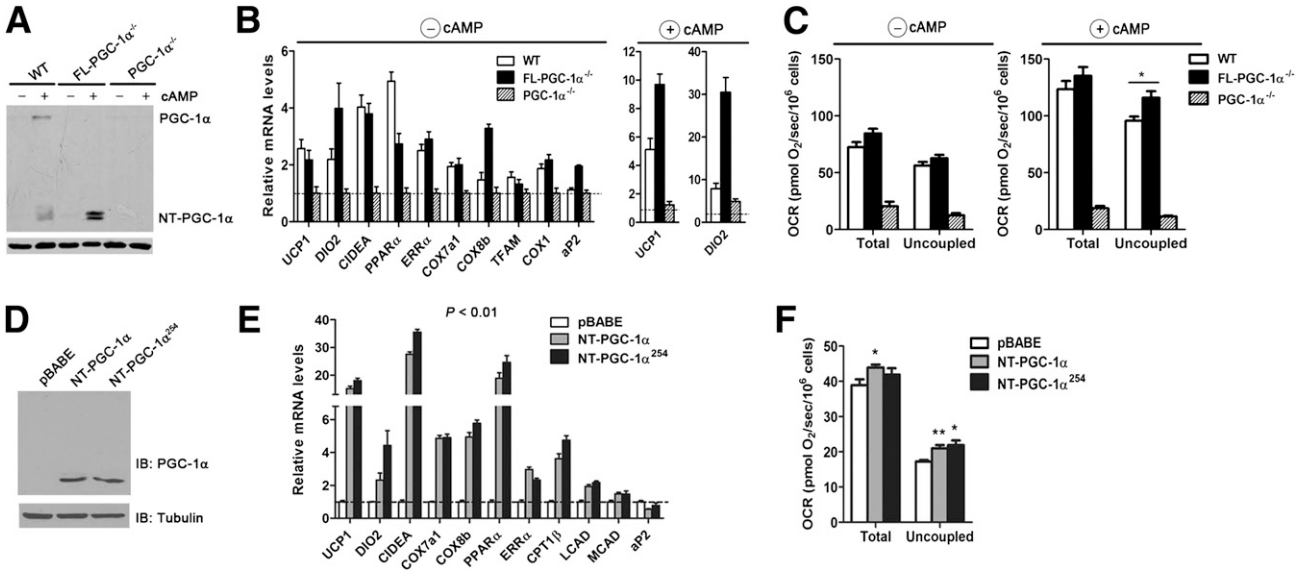

Figure 4—NT-PGC-1α activation enhances thermogenic activity in brown adipocytes. *A*: Protein expression of PGC-1α/NT-PGC-1α and NT-PGC-1α^{254} in differentiated WT, FL-PGC-1α$^{-/-}$, and PGC-1α$^{-/-}$ brown adipocytes treated with vehicle or dibutyryl cAMP for 6 h. *B*: Gene expression analysis of WT, FL-PGC-1α$^{-/-}$, and PGC-1α$^{-/-}$ brown adipocytes treated with vehicle or dibutyryl cAMP for 6 h (n = 5–10 per group). *C*: Oxygen consumption rates of WT, FL-PGC-1α$^{-/-}$, and PGC-1α$^{-/-}$ brown adipocytes (10^6 cells) treated with vehicle or dibutyryl cAMP (n = 12–17 per group). Uncoupled mitochondrial respiration was measured by injection of oligomycin. *D*: Ectopic expression of NT-PGC-1α or NT-PGC-1α^{254} in PGC-1α$^{-/-}$ brown adipocytes by retroviral infection. IB, immunoblot. *E*: Effect of NT-PGC-1α and NT-PGC-1α^{254} on thermogenic and mitochondrial gene expression in PGC-1α$^{-/-}$ brown adipocytes (n = 6 per group). *F*: Effect of NT-PGC-1α and NT-PGC-1α^{254} on total and uncoupled respiration in PGC-1α$^{-/-}$ brown adipocytes (10^6 cells) (n = 5 per group). All data are presented as the mean ± SEM. $^*P < 0.05$, $^{**}P < 0.01$ determined by Student t test. sec, seconds.

genes, and their effect on gene expression was comparable (Fig. 4*E*). Moreover, NT-PGC-1α and NT-PGC-1α^{254} substantially increased both total and uncoupled respiration in PGC-1α$^{-/-}$ brown adipocytes (Fig. 4*F*). These results clearly demonstrate that NT-PGC-1α and NT-PGC-1α^{254} are functionally comparable and directly activate a thermogenic gene program in brown adipocytes.

FL-PGC-1α$^{-/-}$ White Adipose Tissue Exhibits Enhanced Expression of FAO and Lipolytic Genes

Histological analyses showed that adipocytes of epididymal, retroperitoneal, and inguinal fat pads from FL-PGC-1α$^{-/-}$ mice were significantly smaller in size compared with WT controls (Fig. 5*A*). In particular, the greatest difference was observed in inguinal white adipose tissue (IWAT) (Fig. 5*A*). FL-PGC-1α$^{-/-}$ IWAT had a greater frequency of small adipocytes and a lower frequency of mid- to large-sized adipocytes, resulting in a 26% reduction in adipocyte areas (Fig. 5*B*). However, there was no significant change in mitochondrial number in FL-PGC-1α$^{-/-}$ IWAT (data not shown). In line with reduced fat cell size, FL-PGC-1α$^{-/-}$ IWAT displayed decreased triglyceride content compared with WT controls (Fig. 5*D*). Moreover, primary adipocytes isolated from FL-PGC-1α$^{-/-}$ fat depots have the trend toward higher basal and isoproterenol-stimulated lipolysis compared with control adipocytes, although this difference did not reach statistical significance (Fig. 5*C*).

HFD suppresses the expression of PGC-1α, mitochondrial biogenesis, OXPHOS, and FAO genes in adipose tissue (46). As expected, PGC-1α protein expression was below the detectable level (data not shown), but NT-PGC-1α protein was detected with variation in IWAT from HFD-fed WT mice (Fig. 5*F*). On the contrary, NT-PGC-1α^{254} protein was more consistently expressed in FL-PGC-1α$^{-/-}$ IWAT (Fig. 5*F*). Thus, we investigated whether increased NT-PGC-1α^{254} proteins alter the expression of mitochondrial genes involved in OXPHOS and FAO. Gene expression analysis showed that mitochondrial OXPHOS genes and FAO genes including MCAD and LCAD were upregulated by 20–70% in FL-PGC-1α$^{-/-}$ IWAT (Fig. 5*G*). Moreover, adipose triglyceride lipase, the rate-limiting enzyme for adipocyte lipolysis, was significantly upregulated. In contrast, lipogenic genes such as FAS and DGAT2 were downregulated in FL-PGC-1α$^{-/-}$ IWAT (Fig. 5*G*). The expression of UCP1, DIO2, and glucose uptake genes was not different between groups (Fig. 5*G*). Similarly, retroperitoneal WAT exhibited increased expression of genes involved in mitochondrial OXPHOS, FAO, and lipolysis (Fig. 5*H*). Alterations in gene expression were less significant in epididymal FL-PGC-1α$^{-/-}$ WAT, but PPARα and lipolytic genes were consistently upregulated (Fig. 5*I*). Together, these data suggest that enhanced lipid mobilization and oxidation account for the decreased lipid storage in FL-PGC-1α$^{-/-}$ WAT during HFD feeding.

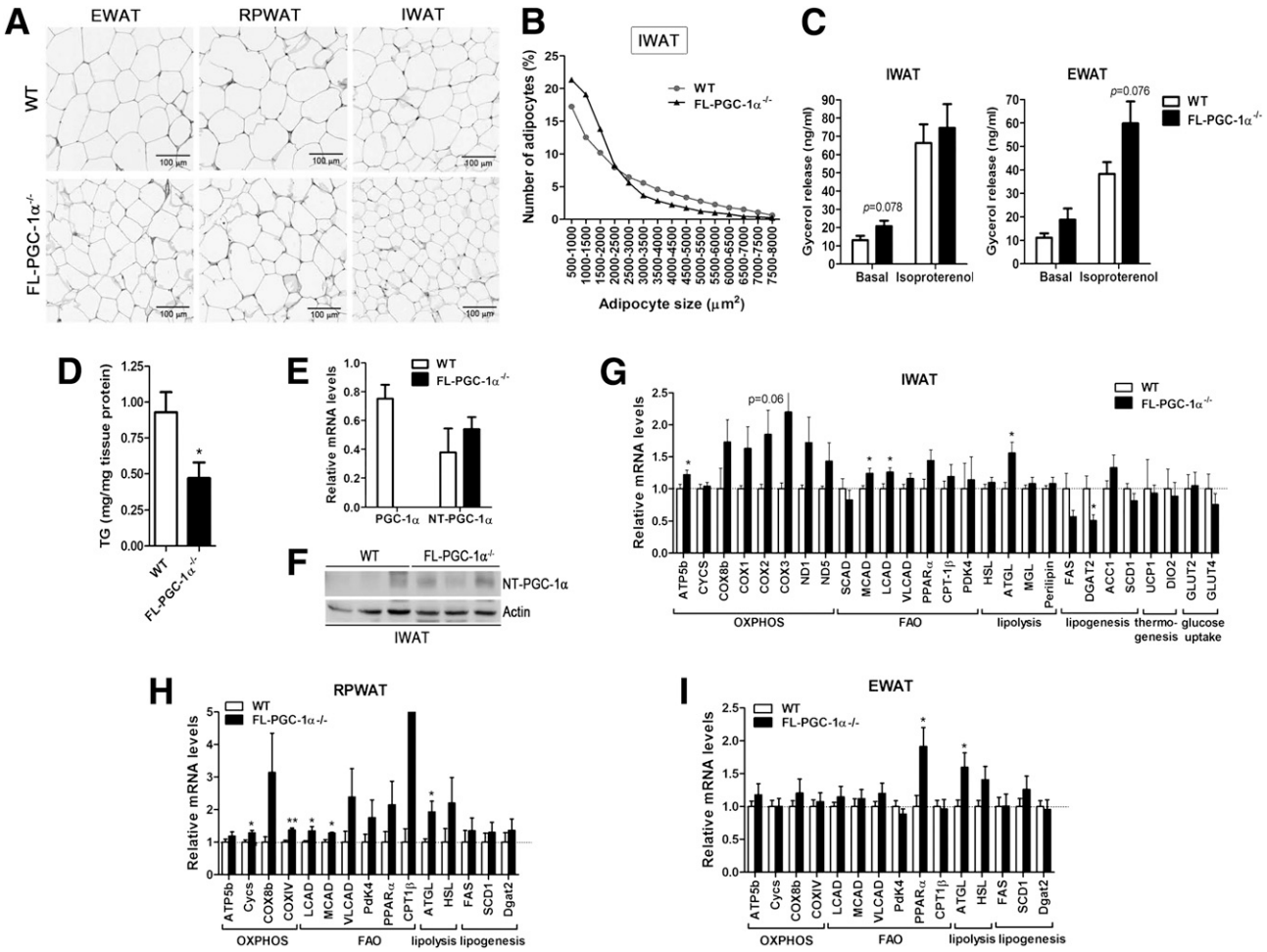

Figure 5—Analysis of white adipose tissue from FL-PGC-1α$^{-/-}$ mice fed HFD. *A*: Representative images of H-E–stained sections of adipose tissues from WT and FL-PGC-1α$^{-/-}$ mice fed HFD for 16 weeks. Scale bar: 100 μm. *B*: Frequency distribution of adipocyte cell size in inguinal adipose tissue from WT and FL-PGC-1α$^{-/-}$ mice fed HFD. *C*: Basal and isoproterenol-stimulated lipolysis of primary adipocytes isolated from inguinal and epididymal fat depots of WT and FL-PGC-1α$^{-/-}$ mice fed HFD for 13 weeks (n = 5 per group). Lipolytic activity was measured in triplicate and represented as glycerol release. *D*: Triglyceride (TG) content of inguinal fat depots from WT and FL-PGC-1α$^{-/-}$ mice fed HFD for 16 weeks (n = 8 per group). *E*: Quantitative real-time PCR analysis of PGC-1α and NT-PGC-1α/NT-PGC-1α^{254} mRNA in inguinal fat from WT and FL-PGC-1α$^{-/-}$ mice fed HFD. *F*: Protein levels of NT-PGC-1α and NT-PGC-1α^{254} in inguinal fat extracts from WT and FL-PGC-1α$^{-/-}$ mice fed HFD, respectively. *G*: Quantitative real-time PCR analysis of mitochondrial OXPHOS, FAO, lipolytic, lipogenic, glucose uptake, and thermogenic genes in inguinal fat from WT and FL-PGC-1α$^{-/-}$ mice fed HFD (n = 6–7 per group). *H* and *I*: Quantitative real-time PCR analysis of mitochondrial OXPHOS, FAO, lipolytic, and lipogenic genes in retroperitoneal (*H*) and epididymal (*I*) fat from WT and FL-PGC-1α$^{-/-}$ mice fed HFD (n = 6–8 per group), respectively. All data are presented as the mean ± SEM. *P < 0.05, **P < 0.01 determined by Student t test. EWAT, epididymal white adipose tissue; RPWAT, retroperitoneal white adipose tissue.

FL-PGC-1α$^{-/-}$ Mice Are Protected From HFD-Induced Hepatic Steatosis

Given that FL-PGC-1α$^{-/-}$ mice fed HFD showed a significant reduction in liver weights (Fig. 1*F*), we examined liver sections from WT and FL-PGC-1α$^{-/-}$ mice fed HFD. WT mice developed hepatic steatosis as evidenced by accumulation of large lipid droplets in liver (Fig. 6*A*). In contrast, the liver from FL-PGC-1α$^{-/-}$ mice had fewer and smaller lipid droplets, in correlation with reduced hepatic triglyceride content confirmed by triglyceride quantification (Fig. 6*B*). Gene expression analysis revealed that mRNA levels of lipogenic genes FAS and SCD1 were ~40% lower in FL-PGC-1α$^{-/-}$ livers (Fig. 6*C*). Consistently, FL-PGC-1α$^{-/-}$ livers exhibited reduced expression of FAS and SCD1 proteins compared with WT controls (Fig. 6*D*), suggesting that a decrease in lipogenesis partly contributes to the attenuation of hepatic lipid accumulation.

DISCUSSION

During prolonged activation of adipose tissue by cold or β-adrenergic receptor agonist, PGC-1α and NT-PGC-1α play a crucial role in adaptive thermogenesis by activating a thermogenic gene program in BAT as well as in white adipose tissue undergoing brown remodeling (28–30).

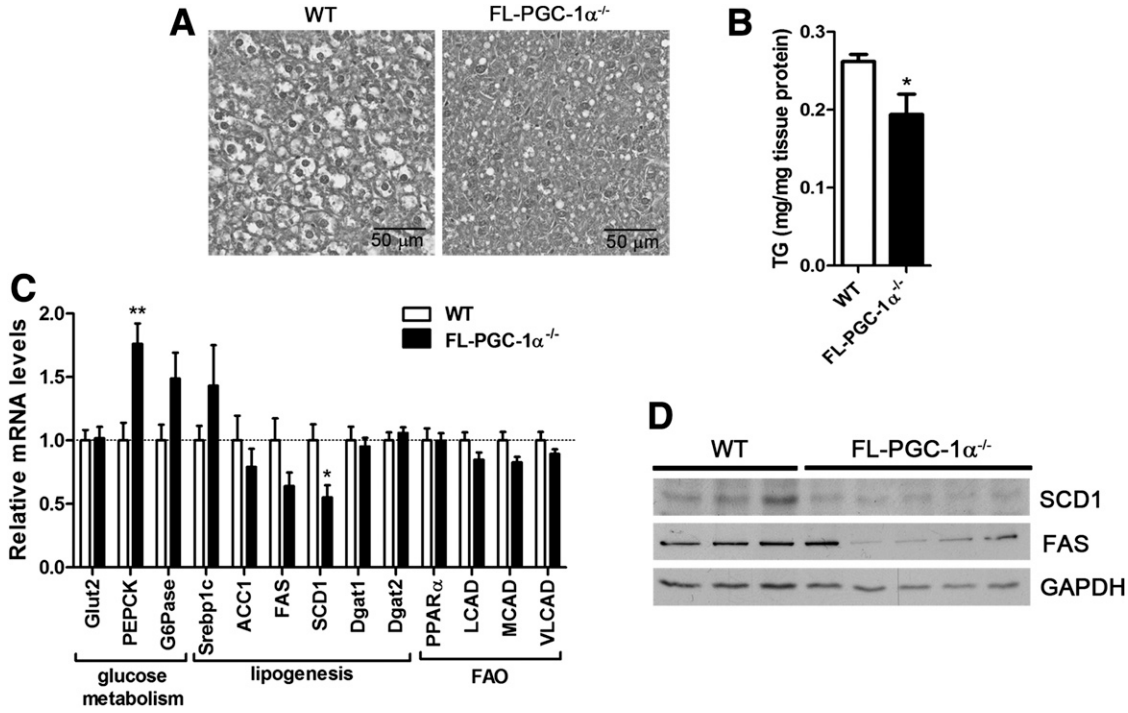

Figure 6—Decreased ectopic fat deposition in FL-PGC-1$\alpha^{-/-}$ liver. *A*: Representative images of H-E–stained sections of livers from WT and FL-PGC-1$\alpha^{-/-}$ mice fed HFD for 16 weeks. Scale bar: 50 μm. *B*: Triglyceride (TG) content of livers from WT and FL-PGC-1$\alpha^{-/-}$ mice fed HFD (n = 8 per group). *C*: Quantitative real-time PCR analysis of glucose metabolism, FAO, and lipogenic genes in livers from WT and FL-PGC-1$\alpha^{-/-}$ mice fed HFD (n = 8 per group). *D*: Western blot analysis of SCD1 and FAS proteins in liver extracts from WT and FL-PGC-1$\alpha^{-/-}$ mice fed HFD. All data are presented as the mean ± SEM. *P < 0.05, **P < 0.01 determined by Student t test.

FL-PGC-1α is dispensable for cold-induced thermogenesis in FL-PGC-1$\alpha^{-/-}$ mice, since NT-PGC-1α^{254}, a functionally equivalent form of NT-PGC-1α, can activate the thermogenic gene program in the absence of PGC-1α during a cold challenge. In the current study, we discovered that FL-PGC-1$\alpha^{-/-}$ mice are relatively resistant to diet-induced obesity under high-fat feeding. FL-PGC-1$\alpha^{-/-}$ mice exhibited a significant reduction in adiposity compared with WT mice. This lean phenotype was not due to alteration in either food intake or physical activity. Instead, FL-PGC-1$\alpha^{-/-}$ mice oxidized more fat by a greater reliance on FAO and expended more energy by BAT-mediated thermogenesis.

At the molecular level, FL-PGC-1$\alpha^{-/-}$ BAT had an increased capacity to oxidize fatty acids without altering FAO gene expression. In line with this, FL-PGC-1$\alpha^{-/-}$ BAT had a preference for fatty acids as a substrate of mitochondrial respiration. Moreover, FL-PGC-1$\alpha^{-/-}$ BAT had an increased ability to dissipate energy as heat by UCP1-mediated uncoupling in accordance with increased expression of UCP1. Given that UCP1 dissipates the proton gradient (chemical energy) by facilitating proton leak across the inner mitochondrial membrane, we speculate that FL-PGC-1$\alpha^{-/-}$ BAT might accelerate FAO to supply a constant flow of energy required for UCP1-mediated energy dissipation. We found that NT-PGC-1α^{254} protein was abundant in HFD-fed FL-PGC-1$\alpha^{-/-}$ BAT compared with WT controls. Since NT-PGC-1α^{254} directly induces the expression of UCP1 in PGC-1$\alpha^{-/-}$ brown adipocytes, these data suggest that elevated levels of NT-PGC-1α^{254} directly affect UCP1 upregulation in HFD-fed FL-PGC-1$\alpha^{-/-}$ BAT. Together, we speculate that a small increase in UCP1-mediated energy dissipation coupled with increased FAO has led to a large impact on body composition over time in FL-PGC-1$\alpha^{-/-}$ mice on HFD. PGC-1$\alpha^{-/-}$ mice deficient in both PGC-1α and NT-PGC-1α have been shown to be resistant to HFD-induced obesity. However, this lean phenotype mainly results from central nervous system–linked hyperactivity rather than diet-induced BAT thermogenesis (32). PGC-1$\alpha^{-/-}$ BATs have an impaired ability to induce UCP1-mediated thermogenesis during cold stress (32).

Type II iodothyronine deiodinase (DIO2) plays a critical role in cold- and diet-induced thermogenesis in BAT (43–45). Induction of DIO2 in BAT triggers rapid conversion of T_4 to the biologically active T_3, thus increasing local thyroid hormone signaling that is critical for the expression of T_3-dependent genes required for thermogenesis (UCP1) and mitochondrial respiration (47). Bile acids have been shown to increase DIO2 expression in BAT, enhancing EE and protecting mice from HFD-induced obesity (23). Thus, our data here suggest that elevated intracellular thyroid hormone signaling by DIO2 upregulation might contribute to the subsequent upregulation of UCP1

and enhanced thermogenic activity in FL-PGC-1$\alpha^{-/-}$ BAT. It is unlikely that DIO2 upregulation in FL-PGC-1$\alpha^{-/-}$ BAT results from increased SNS/β-adrenergic receptor/cAMP signaling, since neither Adrb3 nor NT-PGC-1α, which is a cAMP-responsive gene, was upregulated in FL-PGC-1$\alpha^{-/-}$ BAT. Although cAMP/PKA-activated CREB primarily promotes the transcription of DIO2, thyroid hormone receptor agonists can also induce DIO2 gene expression in brown adipocytes (48), implying a positive feedback loop between DIO2 and T_3-activated thyroid hormone receptors. Given that ectopic expression of NT-PGC-1α^{254} induces DIO2 expression in PGC-1$\alpha^{-/-}$ brown adipocytes, we speculate that NT-PGC-1α^{254} might directly regulate DIO2 gene expression in FL-PGC-1$\alpha^{-/-}$ BAT by coactivating thyroid hormone receptors, although recruitment of NT-PGC-1α^{254} to the DIO2 promoter needs to be determined.

In agreement with an increase in FAO and EE, FL-PGC-1$\alpha^{-/-}$ mice decreased fat storage in adipose tissue and ectopic fat deposition in liver on HFD. Furthermore, FL-PGC-1$\alpha^{-/-}$ adipose tissue depots contained smaller fat cells with reduced triglyceride content. Loss of PGC-1α and NT-PGC-1α has been shown to reduce expression of UCP1, OXPHOS, and FAO genes in PGC-1$\alpha^{-/-}$ white adipose tissue (49). On the contrary, FL-PGC-1$\alpha^{-/-}$ white adipose tissue showed increased expression of genes involved in mitochondrial OXPHOS, FAO, and lipolysis. Given that NT-PGC-1α^{254} proteins were abundantly expressed in FL-PGC-1$\alpha^{-/-}$ adipose tissue compared with WT controls, we speculate that NT-PGC-1α^{254} activation augments the ability of adipose tissue to mobilize and oxidize lipids.

In conclusion, our studies provide compelling evidence for the protective effect of NT-PGC-1α^{254}, which is functionally equivalent to NT-PGC-1α, on HFD-induced obesity by promoting diet-induced thermogenesis and FAO. Importantly, NT-PGC-1α is also produced from the human PGC-1α gene that contains the intronic sequences spanning an alternative splice site for NT-PGC-1α (28,50). Thus, these data suggest that activation of NT-PGC-1α in adipose tissue has therapeutic potential to counteract obesity by increasing BAT-mediated EE and modulating adipose tissue oxidative metabolism.

Acknowledgments. The authors thank Drs. Dan Kelly (Sanford-Burnham Medical Research Institute) and Bruce Spiegelman (Dana-Farber Cancer Institute) for providing FL-PGC-1$\alpha^{-/-}$ mice and PGC-1$\alpha^{-/-}$ brown preadipocytes, respectively. The authors also thank Dr. Thomas Gettys (Pennington Biomedical Research Center) for helpful discussions; Dr. David Burk, Jeho Shin, and Manda Orgeron for their technical contributions and advice; and Cindi Tramonte for excellent administrative support.

Funding. This work was supported by National Institutes of Health grants NIH8 P20-GM103528 (to R.C.N. and J.S.C.), R01-DK-098687-01 (to R.C.N.), and 2P30-DK-072476 (to R.C.N. and J.S.C.). This work used Cell Biology and Bioimaging and Genomics core facilities that are supported in part by Centers of Biomedical Research Excellence (NIH8 P20-GM103528) and Nutrition Obesity Research Centers (2P30-DK-072476) grants from the National Institutes of Health.

Duality of Interest. No potential conflicts of interest relevant to this article were reported.

Author Contributions. H.-J.J. researched data and contributed to the experimental design and discussion. Y.J. researched data. Y.P. researched data and contributed to the experimental design and discussion. R.C.N. contributed to the experimental design and discussion. J.S.C. researched data, contributed to the experimental design and discussion, and wrote the manuscript. J.S.C. is the guarantor of this work and, as such, had full access to all the data in the study and takes responsibility for the integrity of the data and the accuracy of the data analysis.

References

1. Nedergaard J, Golozoubova V, Matthias A, Asadi A, Jacobsson A, Cannon B. UCP1: the only protein able to mediate adaptive non-shivering thermogenesis and metabolic inefficiency. Biochim Biophys Acta 2001;1504:82–106
2. Golozoubova V, Hohtola E, Matthias A, Jacobsson A, Cannon B, Nedergaard J. Only UCP1 can mediate adaptive nonshivering thermogenesis in the cold. FASEB J 2001;15:2048–2050
3. Bartelt A, Bruns OT, Reimer R, et al. Brown adipose tissue activity controls triglyceride clearance. Nat Med 2011;17:200–205
4. Shimizu Y, Nikami H, Saito M. Sympathetic activation of glucose utilization in brown adipose tissue in rats. J Biochem 1991;110:688–692
5. Vallerand AL, Pérusse F, Bukowiecki LJ. Stimulatory effects of cold exposure and cold acclimation on glucose uptake in rat peripheral tissues. Am J Physiol 1990;259:R1043–R1049
6. Cypess AM, Lehman S, Williams G, et al. Identification and importance of brown adipose tissue in adult humans. N Engl J Med 2009;360:1509–1517
7. Virtanen KA, Lidell ME, Orava J, et al. Functional brown adipose tissue in healthy adults. N Engl J Med 2009;360:1518–1525
8. Saito M, Okamatsu-Ogura Y, Matsushita M, et al. High incidence of metabolically active brown adipose tissue in healthy adult humans: effects of cold exposure and adiposity. Diabetes 2009;58:1526–1531
9. Nedergaard J, Bengtsson T, Cannon B. Unexpected evidence for active brown adipose tissue in adult humans. Am J Physiol Endocrinol Metab 2007;293:E444–E452
10. Ouellet V, Labbé SM, Blondin DP, et al. Brown adipose tissue oxidative metabolism contributes to energy expenditure during acute cold exposure in humans. J Clin Invest 2012;122:545–552
11. van der Lans AA, Hoeks J, Brans B, et al. Cold acclimation recruits human brown fat and increases nonshivering thermogenesis. J Clin Invest 2013;123:3395–3403
12. Ouellet V, Routhier-Labadie A, Bellemare W, et al. Outdoor temperature, age, sex, body mass index, and diabetic status determine the prevalence, mass, and glucose-uptake activity of ^{18}F-FDG-detected BAT in humans. J Clin Endocrinol Metab 2011;96:192–199
13. Cannon B, Nedergaard J. Brown adipose tissue: function and physiological significance. Physiol Rev 2004;84:277–359
14. Rothwell NJ, Stock MJ. A role for brown adipose tissue in diet-induced thermogenesis. Nature 1979;281:31–35
15. Himms-Hagen J. Brown adipose tissue thermogenesis: interdisciplinary studies. FASEB J 1990;4:2890–2898
16. Bachman ES, Dhillon H, Zhang CY, et al. betaAR signaling required for diet-induced thermogenesis and obesity resistance. Science 2002;297:843–845
17. Hamann A, Flier JS, Lowell BB. Decreased brown fat markedly enhances susceptibility to diet-induced obesity, diabetes, and hyperlipidemia. Endocrinology 1996;137:21–29
18. Feldmann HM, Golozoubova V, Cannon B, Nedergaard J. UCP1 ablation induces obesity and abolishes diet-induced thermogenesis in mice exempt from thermal stress by living at thermoneutrality. Cell Metab 2009;9:203–209
19. Landsberg L, Saville ME, Young JB. Sympathoadrenal system and regulation of thermogenesis. Am J Physiol 1984;247:E181–E189

20. Lowell BB, S-Susulic V, Hamann A, et al. Development of obesity in transgenic mice after genetic ablation of brown adipose tissue. Nature 1993;366:740–742
21. Kontani Y, Wang Y, Kimura K, et al. UCP1 deficiency increases susceptibility to diet-induced obesity with age. Aging Cell 2005;4:147–155
22. Kopecky J, Clarke G, Enerbäck S, Spiegelman B, Kozak LP. Expression of the mitochondrial uncoupling protein gene from the aP2 gene promoter prevents genetic obesity. J Clin Invest 1995;96:2914–2923
23. Watanabe M, Houten SM, Mataki C, et al. Bile acids induce energy expenditure by promoting intracellular thyroid hormone activation. Nature 2006;439:484–489
24. Kharitonenkov A, Shiyanova TL, Koester A, et al. FGF-21 as a novel metabolic regulator. J Clin Invest 2005;115:1627–1635
25. Xu J, Lloyd DJ, Hale C, et al. Fibroblast growth factor 21 reverses hepatic steatosis, increases energy expenditure, and improves insulin sensitivity in diet-induced obese mice. Diabetes 2009;58:250–259
26. Puigserver P, Wu Z, Park CW, Graves R, Wright M, Spiegelman BM. A cold-inducible coactivator of nuclear receptors linked to adaptive thermogenesis. Cell 1998;92:829–839
27. Wu Z, Puigserver P, Andersson U, et al. Mechanisms controlling mitochondrial biogenesis and respiration through the thermogenic coactivator PGC-1. Cell 1999;98:115–124
28. Zhang Y, Huypens P, Adamson AW, et al. Alternative mRNA splicing produces a novel biologically active short isoform of PGC-1alpha. J Biol Chem 2009;284:32813–32826
29. Chang JS, Huypens P, Zhang Y, Black C, Kralli A, Gettys TW. Regulation of NT-PGC-1alpha subcellular localization and function by protein kinase A-dependent modulation of nuclear export by CRM1. J Biol Chem 2010;285:18039–18050
30. Chang JS, Fernand V, Zhang Y, et al. NT-PGC-1α protein is sufficient to link β3-adrenergic receptor activation to transcriptional and physiological components of adaptive thermogenesis. J Biol Chem 2012;287:9100–9111
31. Jun HJ, Gettys TW, Chang JS. Transcriptional activity of PGC-1α and NT-PGC-1α is differentially regulated by twist-1 in brown fat metabolism. PPAR Res 2012;2012:320454
32. Lin J, Wu PH, Tarr PT, et al. Defects in adaptive energy metabolism with CNS-linked hyperactivity in PGC-1alpha null mice. Cell 2004;119:121–135
33. Himms-Hagen J, Melnyk A, Zingaretti MC, Ceresi E, Barbatelli G, Cinti S. Multilocular fat cells in WAT of CL-316243-treated rats derive directly from white adipocytes. Am J Physiol Cell Physiol 2000;279:C670–C681
34. Cousin B, Cinti S, Morroni M, et al. Occurrence of brown adipocytes in rat white adipose tissue: molecular and morphological characterization. J Cell Sci 1992;103:931–942
35. Tiraby C, Tavernier G, Lefort C, et al. Acquirement of brown fat cell features by human white adipocytes. J Biol Chem 2003;278:33370–33376
36. Leone TC, Lehman JJ, Finck BN, et al. PGC-1alpha deficiency causes multi-system energy metabolic derangements: muscle dysfunction, abnormal weight control and hepatic steatosis. PLoS Biol 2005;3:e101
37. Cannon B, Nedergaard J. Respiratory and thermogenic capacities of cells and mitochondria from brown and white adipose tissue. Methods Mol Biol 2001;155:295–303
38. Noland RC, Woodlief TL, Whitfield BR, et al. Peroxisomal-mitochondrial oxidation in a rodent model of obesity-associated insulin resistance. Am J Physiol Endocrinol Metab 2007;293:E986–E1001
39. Schindelin J, Arganda-Carreras I, Frise E, et al. Fiji: an open-source platform for biological-image analysis. Nat Methods 2012;9:676–682
40. Kaiyala KJ, Morton GJ, Leroux BG, Ogimoto K, Wisse B, Schwartz MW. Identification of body fat mass as a major determinant of metabolic rate in mice. Diabetes 2010;59:1657–1666
41. Kaiyala KJ, Schwartz MW. Toward a more complete (and less controversial) understanding of energy expenditure and its role in obesity pathogenesis. Diabetes 2011;60:17–23
42. Tschöp MH, Speakman JR, Arch JR, et al. A guide to analysis of mouse energy metabolism. Nat Methods 2012;9:57–63
43. de Jesus LA, Carvalho SD, Ribeiro MO, et al. The type 2 iodothyronine deiodinase is essential for adaptive thermogenesis in brown adipose tissue. J Clin Invest 2001;108:1379–1385
44. Marsili A, Aguayo-Mazzucato C, Chen T, et al. Mice with a targeted deletion of the type 2 deiodinase are insulin resistant and susceptible to diet induced obesity. PLoS ONE 2011;6:e20832
45. Castillo M, Hall JA, Correa-Medina M, et al. Disruption of thyroid hormone activation in type 2 deiodinase knockout mice causes obesity with glucose intolerance and liver steatosis only at thermoneutrality. Diabetes 2011;60:1082–1089
46. Rong JX, Qiu Y, Hansen MK, et al. Adipose mitochondrial biogenesis is suppressed in db/db and high-fat diet-fed mice and improved by rosiglitazone. Diabetes 2007;56:1751–1760
47. Weitzel JM, Iwen KA, Seitz HJ. Regulation of mitochondrial biogenesis by thyroid hormone. Exp Physiol 2003;88:121–128
48. Martinez de Mena R, Scanlan TS, Obregon MJ. The T3 receptor beta1 isoform regulates UCP1 and D2 deiodinase in rat brown adipocytes. Endocrinology 2010;151:5074–5083
49. Kleiner S, Mepani RJ, Laznik D, et al. Development of insulin resistance in mice lacking PGC-1α in adipose tissues. Proc Natl Acad Sci U S A 2012;109:9635–9640
50. Ydfors M, Fischer H, Mascher H, Blomstrand E, Norrbom J, Gustafsson T. The truncated splice variants, NT-PGC-1α and PGC-1α4, increase with both endurance and resistance exercise in human skeletal muscle. Physiol Rep 2013;1:e00140